Figure S1. MS$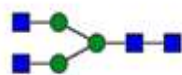^{E}$ spectrum of SWT7 derived HA glycopeptide, *m/z* 3858.62 [M+H]+ (Hex$_8$HexNAc$_2$)LYQNPTTYISVGTSTLNQR, containing site 4. The colors in the figure indicate the following: red-y ions; blue-b ions; green-y/b ions after neutral loss; gray-unassigned ions by the Biopharmalynx. Monosaccharide symbols: ■, N-acetylglucosamine; ●, mannose. Peptide fragments with glycosyl neutral loss are indicated.

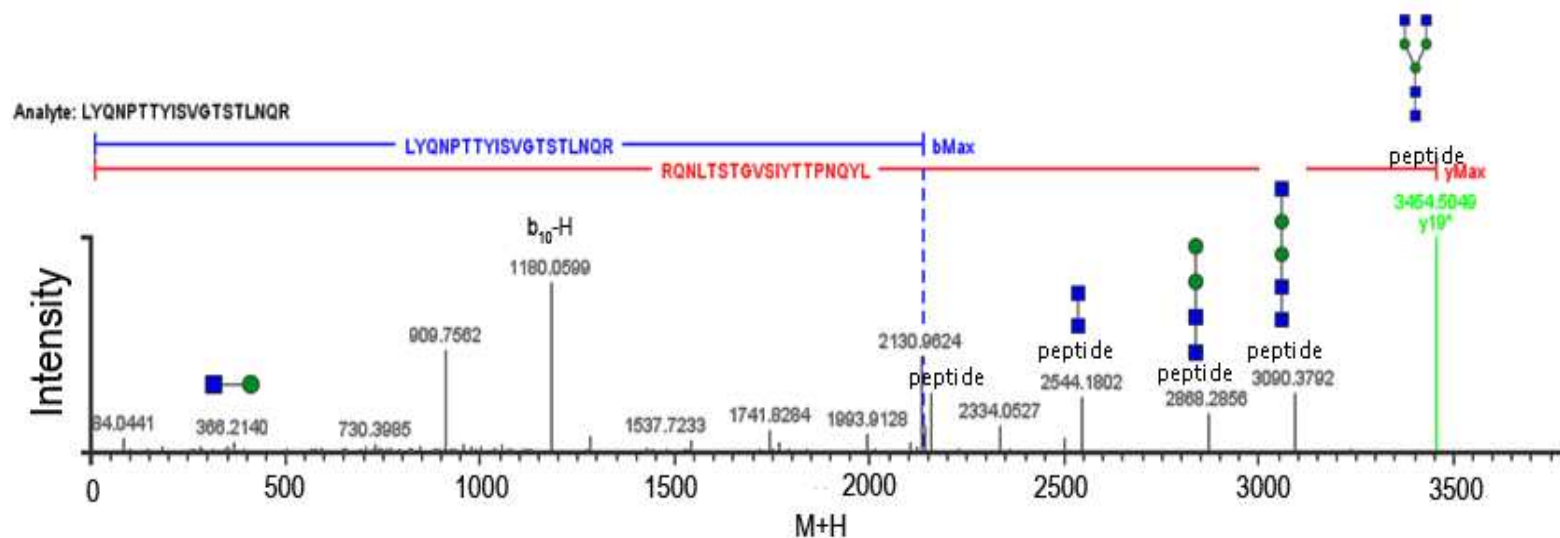Figure S2. MS^E spectrum of SWT7 derived HA glycopeptide, *m/z* 3454.50 [M+H]+ (Hex$_3$HexNAc$_4$)LYQNPTTYISVGTSTLNQR, containing site 4. The colors in the figure indicate the following: red, y ions; blue, b ions; green, y/b ions after neutral loss; gray-unassigned ions by the Biopharmalynx or manually assigned as indicated. Monosaccharide symbols: ■, N-acetylglucosamine; ●, mannose. Peptide fragments with glycosyl neutral loss are indicated.
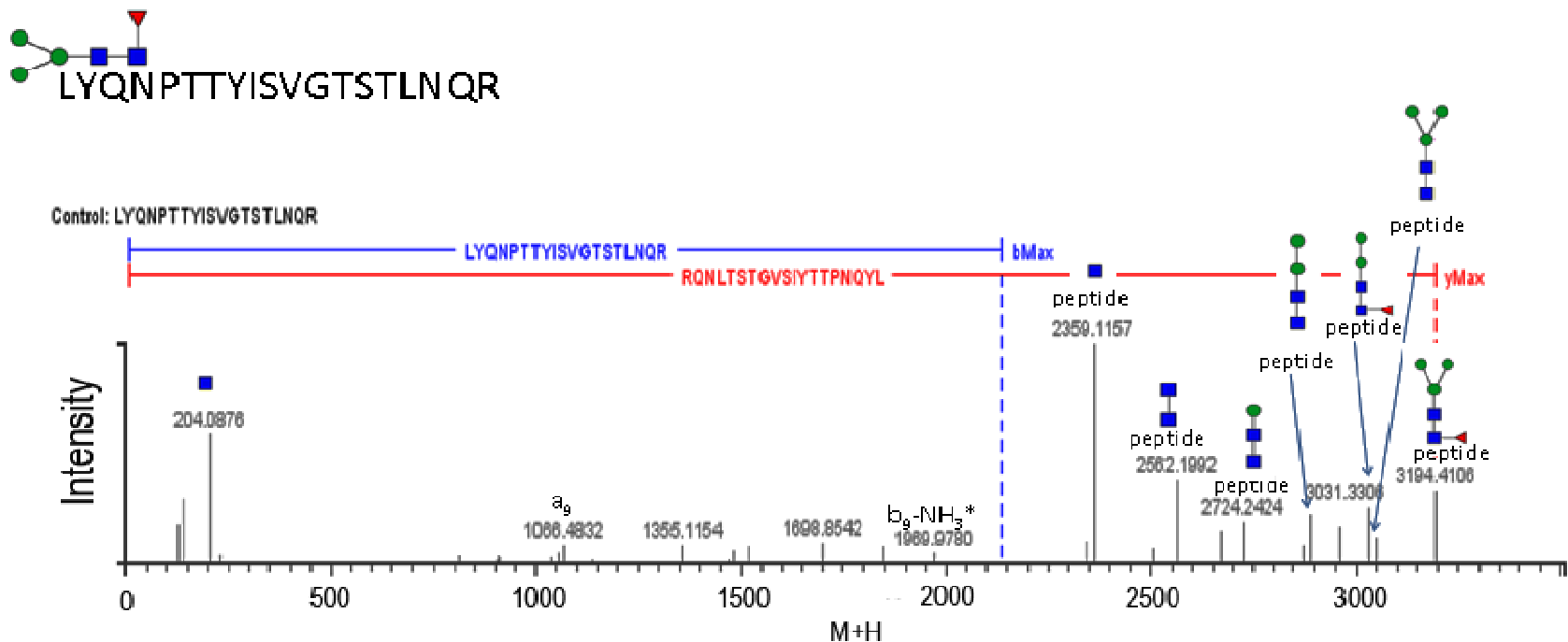
Figure S3. MS^E spectrum of HighFive derived HA glycopeptide, *m/z* 3194.41 [M+H]+

(dHex$_1$dHex$_3$HexNAc$_2$)LYQNPTTYISVGTSTLNQR, containing site 4. The colors in the figure indicate the following: red, y ions;

blue, b ions; green, y/b ions after neutral loss; gray, unassigned ions by the Biopharmalynx or manually assigned as indicated.

Monosaccharide symbols: ■ N-acetylglucosamine; ● , mannose; ▲ , fucose. Peptide fragments with glycosyl neutral loss are

indicated.

Figure S4. MS^E spectrum of Sf9 derived HA glycopeptide, *m/z* 3048.35 [M+H]+ (Hex$_3$HexNAc$_2$)LYQNPTTYISVGTSTLNQR, containing site 4. The colors in the figure indicate the following: red, y ions; blue, b ions; green, y/b ions after neutral loss; gray, are unassigned ions by the Biopharmalynx or assigned as indicated. Monosaccharide symbols: ■, N-acetylglucosamine; ●, mannose. Peptide fragments with glycosyl neutral loss are indicated.
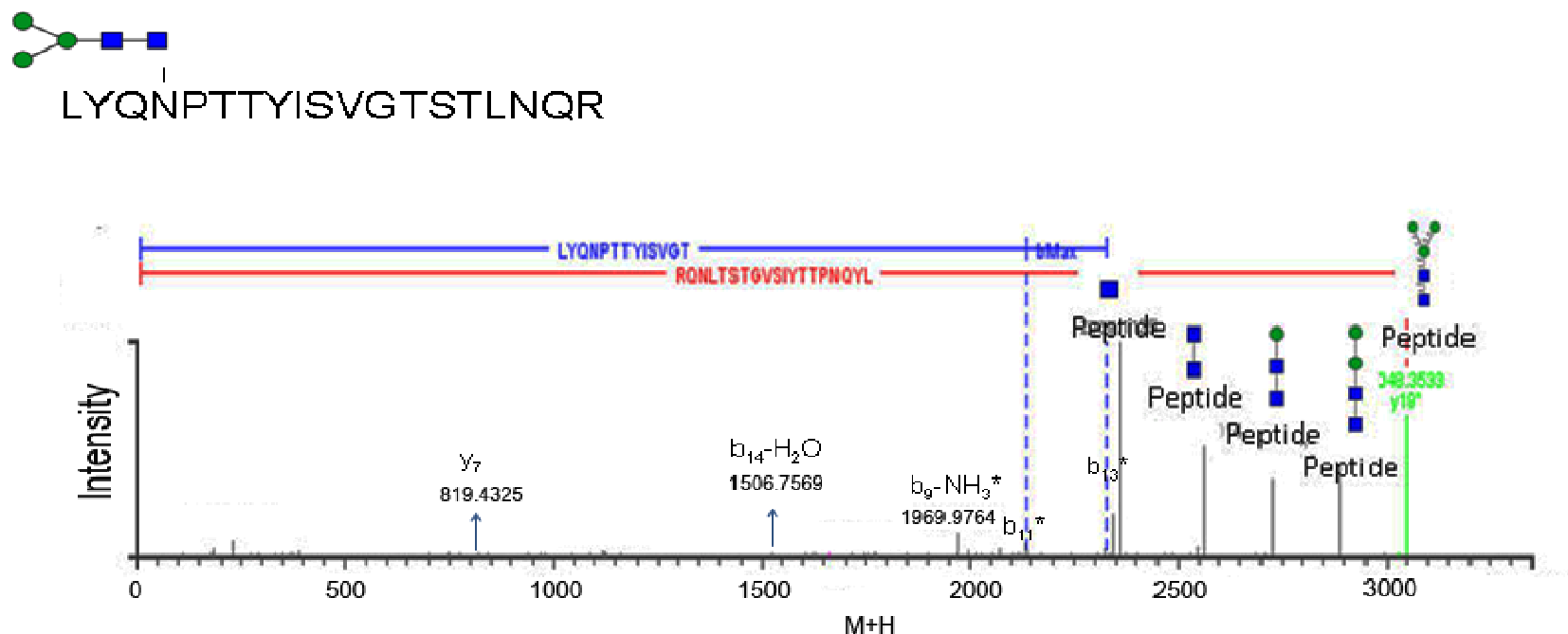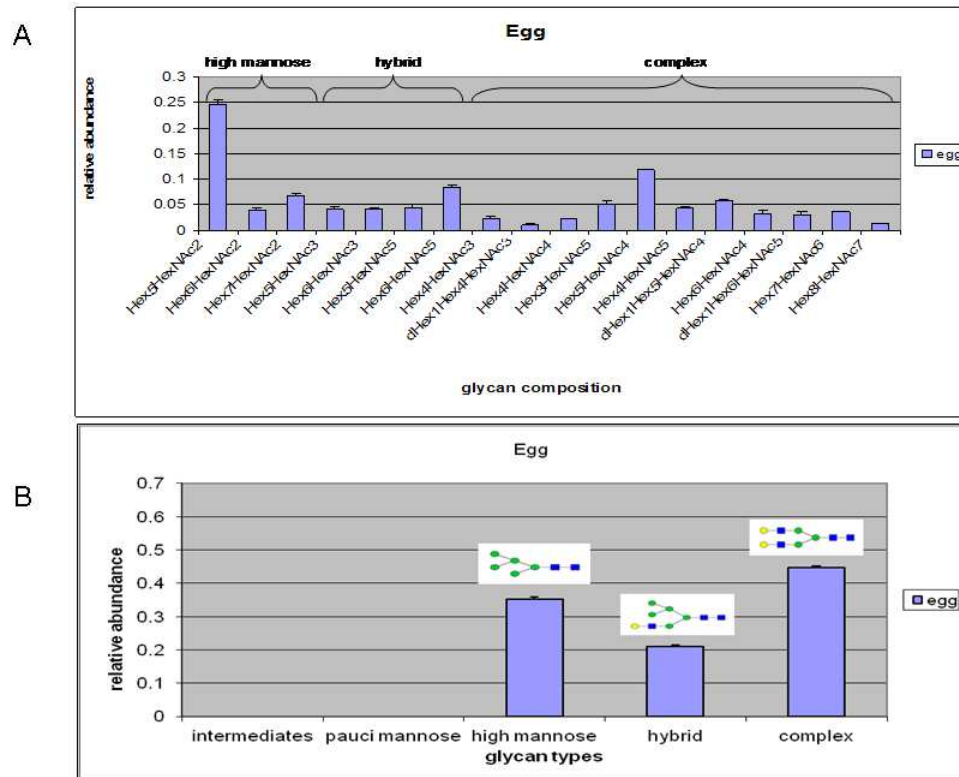
Figure S5. MALDI-TOF MS profile histogram of the egg derived HA released and permethylated glycans. Histograms are grouped by *N*-glycan subtype in A. The subtypes are summed in B for comparison. The inferred composition of the most abundant glycoforms within each sub-group is shown. The summed *N*-glycan subtypes from all cell substrates are shown as a three dimensional plot in

Figure S10. The inferred composition of the most abundant glycoforms within each sub-group is shown. Measurements were performed in triplicate and error bars represent one standard deviation.
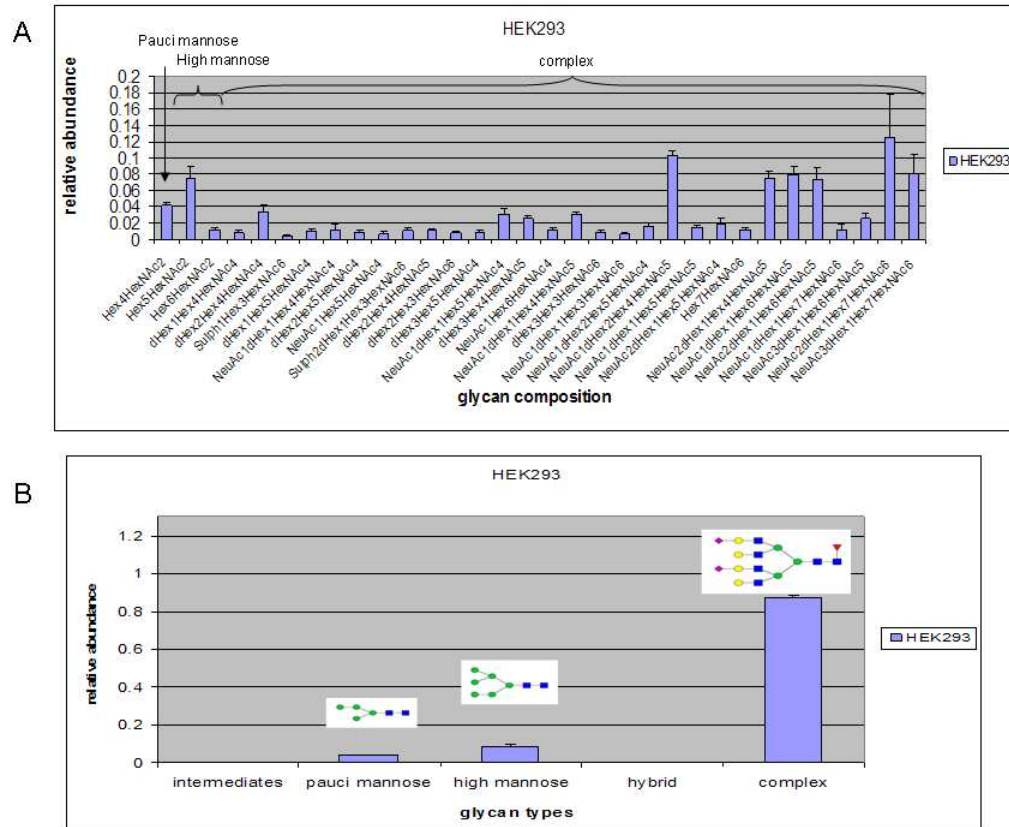
Figure S6. MALDI-TOF MS profile histogram of the HEK293 cell derived HA released and permethylated glycans. Histograms are grouped by *N*-glycan subtype in A. The subtypes are summed in B for comparison. The inferred composition of the most abundant glycoforms within each sub-group is shown. The summed *N*-glycan subtypes from all cell substrates are shown as a three dimensional plot in Figure S10. The inferred composition of the most abundant glycoforms within each sub-group is shown. Measurements were performed in triplicate and error bars represent one standard deviation.
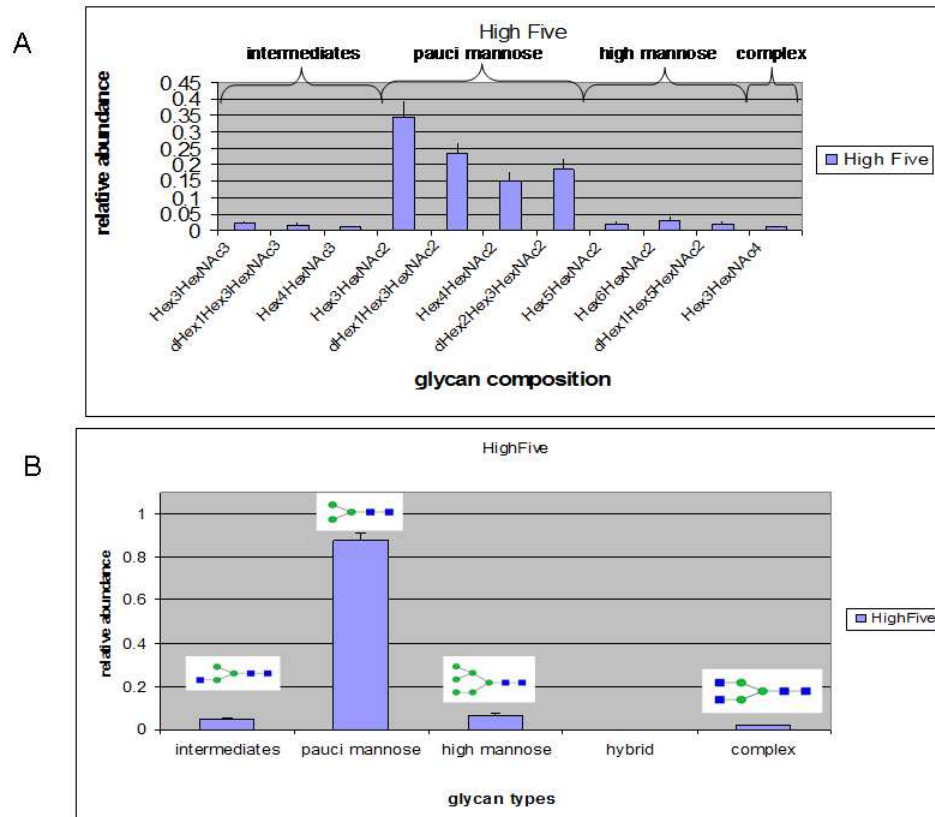
Figure S7. MALDI-TOF MS profile histogram of the HighFive cell derived HA released and permethylated glycans. Histograms are grouped by *N*-glycan subtype in A. The subtypes are summed in B for comparison. The inferred composition of the most abundant glycoforms within each sub-group is shown. The summed *N*-glycan subtypes from all cell substrates are shown as a three dimensional plot in Figure S10. Measurements were performed in triplicate and error bars represent one standard deviation.
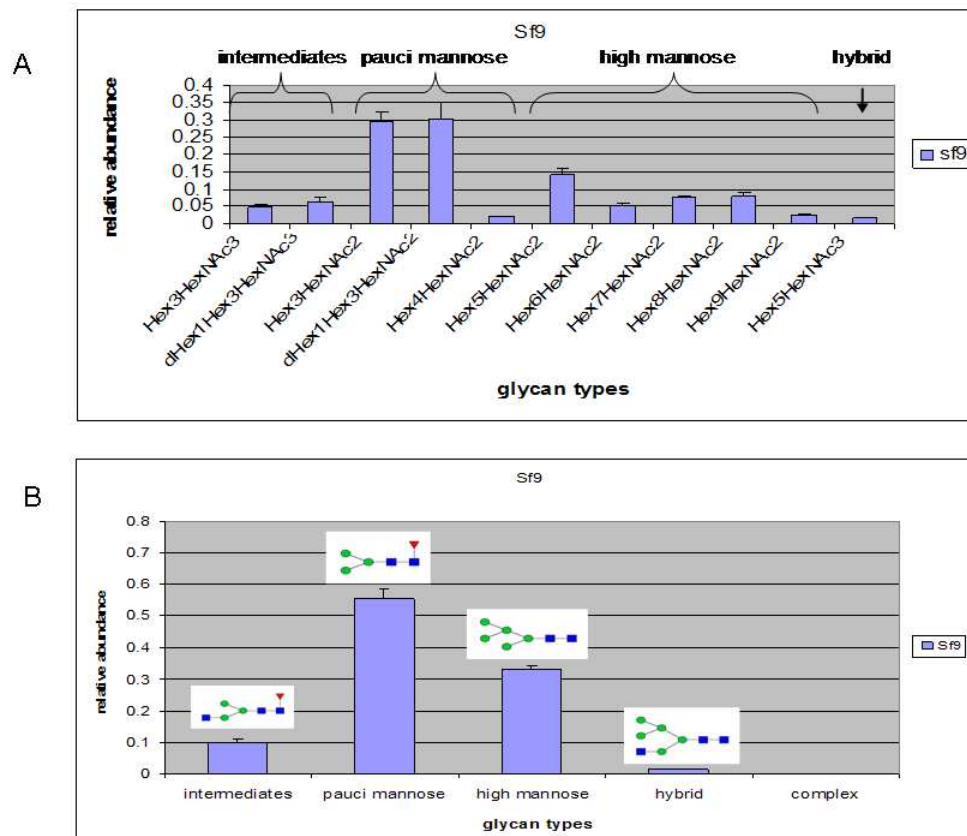
Figure S8. MALDI-TOF MS profile histogram of the Sf9 cell derived HA released and permethylated glycans. Histograms are grouped by *N*-glycan subtype in A. The subtypes are summed in B for comparison. The inferred composition of the most abundant glycoforms within each sub-group is shown. The summed *N*-glycan subtypes from all cell substrates are shown as a three dimensional plot in Figure S10. Measurements were performed in triplicate and error bars represent one standard deviation.
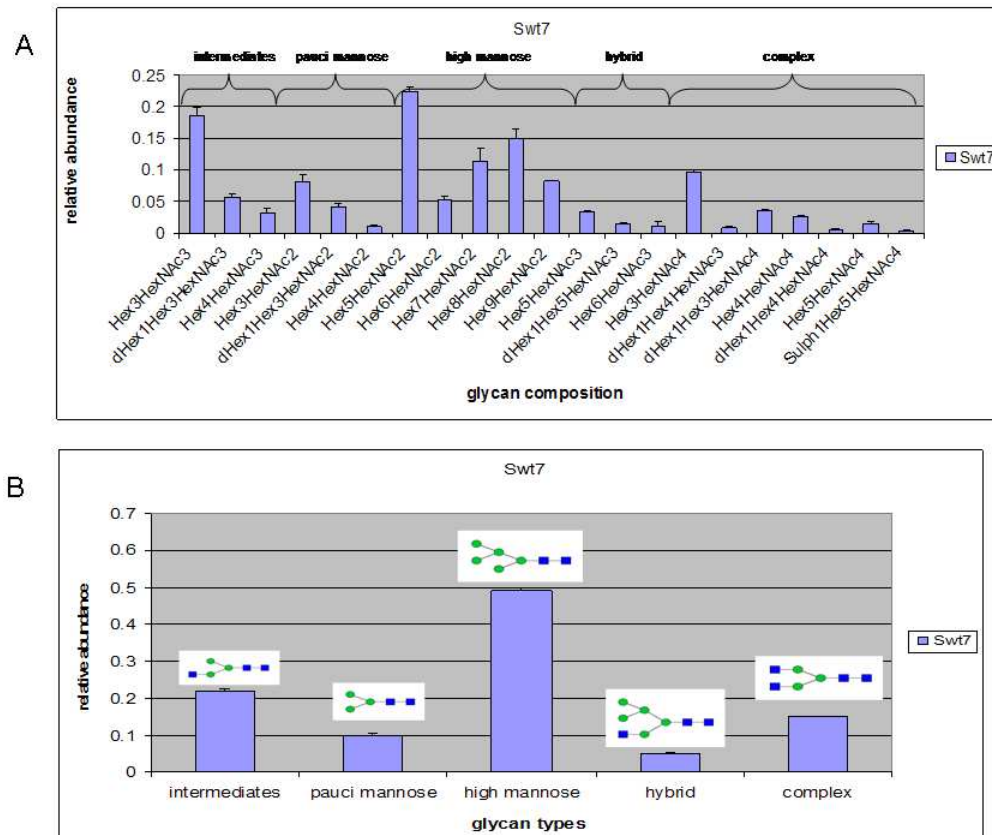
Figure S9. MALDI-TOF MS profile histogram of the SWT7 cell derived HA released and permethylated glycans. Histograms are grouped by *N*-glycan subtype in A. The subtypes are summed in B for comparison. The inferred composition of the most abundant glycoforms within each sub-group is shown. The summed *N*-glycan subtypes from all cell substrates are shown as a three dimensional plot in Figure S10. Measurements were performed in triplicate and error bars represent one standard deviation.
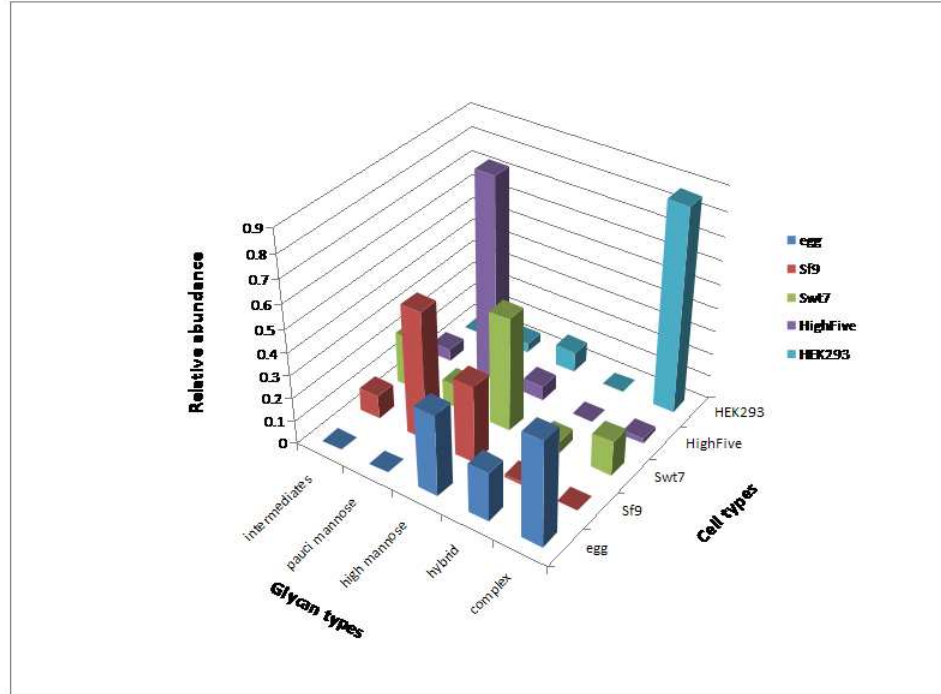
Figure S10. *N*-glycan abundances within subgroups. *N*-glycans present in intermediate, pauci mannose, high mannose, hybrid and complex subgroups are shown for HAs derived from each cell platform.